



RESEARCH ARTICLE

Configuration design of movable heavy-duty reconfigurable posture adjustment platform with dual motion modes

Rui Wang¹ , Xiaoyan Xiong¹, Jinzhu Zhang^{1,2}  and Ruilin Yuan^{1,2}

¹College of Mechanical and Vehicle Engineering, Taiyuan University of Technology, Taiyuan, Shanxi, China

²National Key Laboratory of Metal Forming Technology and Heavy Equipment, Taiyuan, Shanxi, China

Corresponding authors: Xiaoyan Xiong; Email: xiongy7070@163.com; Jinzhu Zhang; Email: zhangjinzhu@tyut.edu.cn

Received: 27 November 2023; **Revised:** 5 March 2024; **Accepted:** 1 April 2024

Keywords: posture adjustment mechanism; dual motion modes; reconfigurable design; coupling sub-chain

Abstract

The existing single-mode posture adjustment equipment for solar wing docking is only suitable for a limited number of satellite dimensions; it could not meet the diverse development trends of satellite models. The working range requirements are different when different-sized satellites dock with the solar wing, and the docking process is divided into two stages in this paper. While the DOFs required for the two stages are different, a movable heavy-load reconfigurable redundant posture adjustment platform (RrPAP) with dual motion modes is proposed in this paper. The RrPAP consists of a wheeled mobile platform and a reconfigurable parallel posture adjustment mechanism (PAM). The micro-motion PAM limb types are synthesized, and the comprehensive load-bearing index is proposed to select the mechanism types for heavy-load conditions. A decentralized four-limb six-degree-of-freedom (6-DOF) parallel micro-motion PAM is designed. In the macro-motion stage, for the PAM to still have a defined motion after being released from ground constraints, a serial coupling sub-chain is designed between adjacent limbs to restrict relative movement between them. A type synthesis method for symmetrically coupled mechanisms based on mechanism decoupling and motion distribution is proposed. Four types of symmetrically coupled mechanisms with multi-loop consisting of serial coupling sub-chains are synthesized by using this method. The feasibility of the proposed method is demonstrated through an example using the constraint synthesis method based on screw theory. This work provides a foundation for subsequent refinement and expansion of type synthesis theories and the selection of new types of mechanisms.

1. Introduction

Solar wing is the primary device that provides spacecraft with electrical power in space, and it is a critical component for ensuring the safety and reliability of spacecraft. Traditional solar wing docking relies on manual alignment, where the three indicators of pitch, yaw, and roll are mutually coupled during the posture adjustment process. This results in complex operations and significant time consumption and severely impacts the reliability and precision of spacecraft assembly. Furthermore, solar wings are large, heavy, and easily folded and have low stiffness, making their docking and installation more difficult. Hence, there is an urgent need for automated installation and docking equipment to enhance solar wing installation's efficiency and precision, which ultimately extends their fault-free service life in orbit.

The mechanism serves as the “skeleton” for solar wing docking equipment, and the functionality and performance of the equipment largely depend on the configuration of the mechanism [1–3]. Parallel mechanisms (PMs), due to their compact structure, high precision, robust rigidity, and substantial load-bearing capacity, have been widely utilized in the aerospace field, particularly in the assembly of large aerospace components. Currently, the mainstream spacecraft posture adjustment mechanism (PAM) is Stewart and its variant configuration [4], such as 6-SPS, 6-UPS, and other PMs [5, 6]. This type of

PM owns multiple limbs and a large structure that takes up a lot of space during large or super-large loads. This has resulted in a large spacecraft assembly production line that is difficult to move and adjust and has impacted the diversified development of satellite models. Compared to non-redundant PMs such as Stewart and its variant configurations, redundant parallel mechanisms (RPMs) are miniaturized in structural/drive when subjected to large or super-large loads [7]. Among various RPM types, the n -PPPS RPMs are widely used in aerospace manufacturing for assembling large components. The 3-PPPS RPM is a common application [8] but may encounter load imbalance issues. The n -PPPS RPMs with $n > 3$, such as the 4-PPPS RPM [9], offer a viable solution to overcome this issue.

With the diversification of satellite models, it is necessary for solar wing docking equipment to possess strong characteristics such as multi-satellite adaptability, modular assembly and disassembly, and the ability to make rapid adjustments in various modes. The traditional PAMs, such as n -SPPP, have a fixed structural form, leading to fixed functionality and application scenarios, which could not meet the demand for docking of different-sized satellites. In contrast, reconfigurable mechanisms exhibit the characteristics of “one machine with multiple functions” and “one machine with multiple uses.” These mechanisms can demonstrate strong adaptability in changing scenarios [10, 11]. Currently, there have been some studies on reconfigurable mechanisms. Dai et al. [12] proposed the concept of metamorphic mechanisms while researching the folding process of paper boxes and handicrafts. To achieve the reconfiguration of reconfigurable mechanisms, a series of methods have been proposed [13, 14], including topological reconfiguration [15], geometric reconfiguration [16], and branching reconfiguration [17]. In addition, Ye [18], Lu [19], and others [20–22] have also conducted related research. Some scholars, for instance, Galletti and Fanghella [23, 24], have extended their work from synthesizing traditional PMs with a single motion mode to achieve reconfigurable PMs with multiple motion modes.

Multi-mode motion mechanisms are often multi-loop coupled mechanisms. However, due to the differences between multi-loop coupled reconfigurable mechanisms and traditional PMs, the mature PM synthesis theories [25–27] are not suitable for this type of mechanism. Therefore, seeking theoretical methods for synthesizing configurations of multi-loop coupled reconfigurable mechanisms is a new direction and challenge in the field of mechanism design. Dai et al. [28] analyzed the mobility of a ball-and-socket toy using constraint loop theory; however, as the number of independent loops increases, the calculations become more complex. Cao et al. [29] synthesized a class of two-layer dual-loop mechanisms based on mobility analysis. Zeng et al. [30] synthesized various multi-loop coupled mechanisms based on mathematical logic and displacement group theory. However, this method is relatively complex. Inspired by Kirchhoff’s current law, Liu et al. proposed a simple and effective method for calculating the DOF of multi-loop coupled mechanisms based on the screw theory; they used it to design and analyze a novel regular triangular double-pyramid mechanism [31]. Similarly, Tian and Fang [32] proposed a systematic approach for synthesizing parallel manipulator structures with coupling sub-chains based on the screw theory and introduced a class of 2R2T and 3T1R generalized PMs [33]. Paul et al. [34] also presented a series of multi-loop coupled mechanisms capable of rolling and crawling motions. Ding et al. [35] designed a class of umbrella-like deployable mechanisms’ topology based on a novel two-layer dual-loop spatial linkage unit and designed a multi-loop coupled mechanism with 6-DOF for forging manipulators. Currently, scholars have focused on exploring the theoretical foundations of reconfigurable mechanism structures but lack the design of reconfigurable mechanisms tailored to practical operational requirements.

During the research process, we discovered that the posture adjustment platform for solar wing docking exhibits discontinuous changes in DOF requirements during operation, that is, the constraints of the mechanism change discontinuously due to state changes, which results in the change of the DOF. Specifically, on the one hand, the posture adjustment platform is required to transport the satellite in a large range of motion in the horizontal plane during docking, which requires the posture adjustment platform to have 3-DOF motion in the plane. On the other hand, a posture adjustment platform is also required to adjust the satellite’s position and posture in a small range, which requires the posture adjustment platform to have 6-DOF motion. Therefore, a dual-mode mechanism is proposed to be used in the design of PAP due to the working range. Based on the dual-mode mechanism, in order to

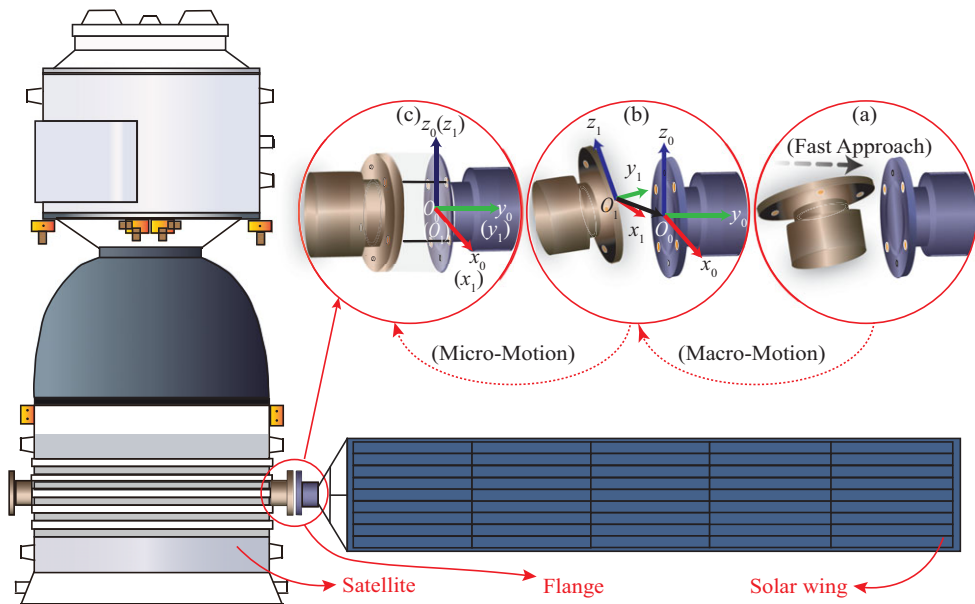


Figure 1. Docking process.

solve the discontinuous change of DOF caused by the discontinuous constraint change during the mode transformation, an RrPAP for adjusting the position and posture of the satellite during the solar wing docking process is proposed in this paper. The paper is organized into four parts: Section 2 introduces the layout design of dual-mode docking and PAM with both macro-motion and micro-motion modes. Section 3 covers configuration design, including cases of decentralized limbs and PMs with coupling sub-chains between limbs. It provides detailed explanations of decentralized limb types and selection criteria, the arrangement of kinematic pairs, the number of driving pairs (DN), and the design method of reconfigurable mechanisms. Section 4 presents the conclusion.

2. Layout design of dual-mode docking and posture adjustment platform

During the docking process of the solar wing and satellite, the solar wing is fixed, and the position and posture of the satellite need to be adjusted in real time by a RrPAP. The docking process can be divided into two stages according to the motion range of the satellite, as shown in Fig. 1. The coordinate systems shown in Fig. 1 are established on the two flanges' end faces, respectively. The origin is the center point of the flange end face, the flange axis is the y -axis, the vertical direction of the connection between the two adjacent dock holes of the flange is the x -axis, and the z -axis is determined by the right-hand rule.

1) Macro-motion stage: the satellite is transported in a large range, as shown in Fig. 1(a) until its docking flange coordinate system is close to that of the solar wing flange, and the satellite is flipped by 90° to enter micro-motion range (O_1 is located in the left hemisphere of O_0 as the center, with a radius of 50 mm and the flange end face of the solar wing as the dividing surface, and each corresponding axis angle is less than 5°), as shown in Fig. 1(b). In this stage, the RrPAP requires at least 3-DOF in the plane.

2) Micro-motion stage: the position and posture of the satellite are adjusted within a small range until the satellite flange coordinate system coincides with the solar wing flange coordinate system, as shown in Fig. 1(c). In this stage, the RrPAP requires 6-DOF to realize position and attitude adjustments.

According to the difference in motion range and accuracy of the two stages, the wheeled mobile platform (WMP) is used in the macro-motion stage, while the PM is used as a PAM in the micro-motion

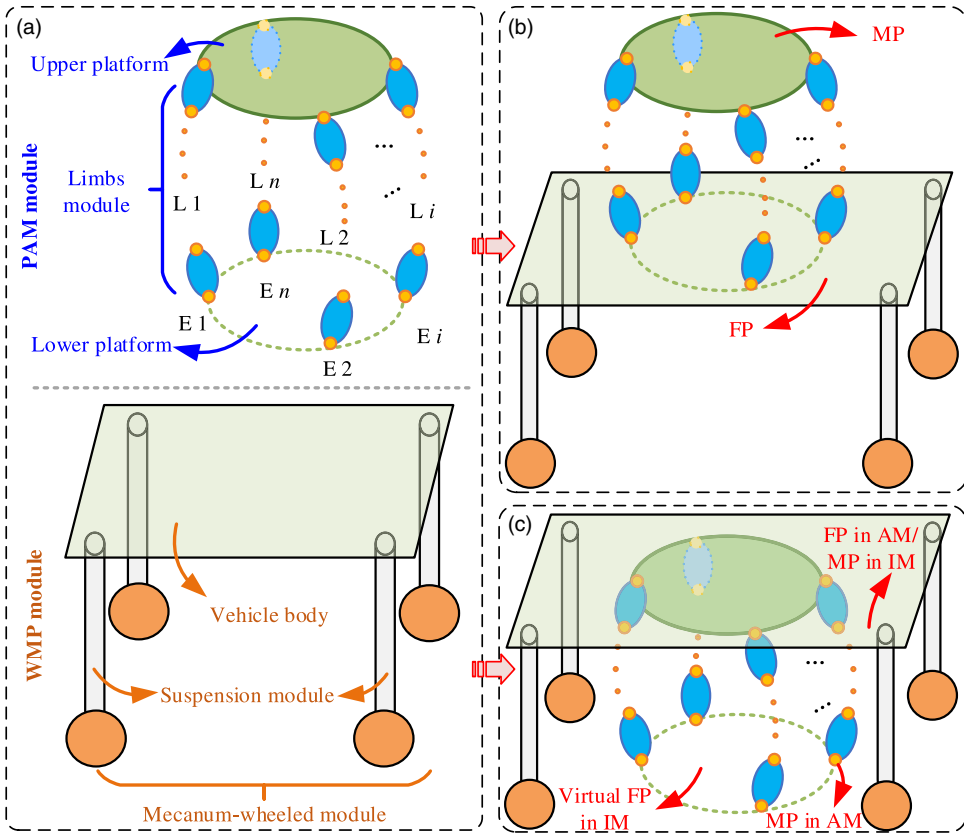


Figure 2. RrPAP layouts. Note: L_i denotes limb i , and E_i denotes the end of limb i . MP denotes the moving platform, and FP denotes the fixed platform. AM denotes macro-motion, and IM denotes micro-motion.

stage; RrPAP consists of WMP and PAM as shown in Fig. 2(a). There are two possibilities for the layout between the WMP and the PAM:

Layout 1: The WMP and the PAM are in series. The vehicle body of the WMP is always the fixed platform of the PAM, and the upper platform of the PAM is the moving platform, as shown in Fig. 2(b).

Layout 2: The WMP and the PAM are in parallel. The vehicle body of the WMP is the fixed platform of the PAM, and it is the moving platform of the PAM in the micro-motion stage, as shown in Fig. 2(c).

By comparing, it can be seen that the RrPAP in layout 1 has a larger overall volume. The stiffness of the RrPAP is low due to the flexible contact between the wheel and the ground. There may be a “virtual leg” that cannot be eliminated, and accuracy cannot be guaranteed. The RrPAP in layout 2 has a compact structure, high stiffness, and good accuracy retention. Although the “virtual leg” phenomenon also exists in the micro-motion stage, it can be eliminated. Therefore, this paper chooses layout 2 to design the RrPAP further.

3. Configuration design of dual-mode posture adjustment mechanism

After obtaining the layout form of the RrPAP, another problem is to clarify the configuration of the WMP and the PAM. The configuration of the WMP is obvious, and a four-Mecanum-wheeled omnidirectional mobile system is adopted in this paper. The configuration of the PAM is diversified, which can be the traditional PM, decentralized limbs parallel mechanism (DLPM), and PM with coupling

Table I. Design index of dual-mode RrPAP.

Design index	Macro-motion	Micro-motion
DOF	3 (2T1R) for WMP 3 (3R) for PAM	6 (3R3T) for PAM
Working range	$x:>50\text{mm}$ $y:>50\text{mm}$	$x:\pm 50\text{ mm}, y:\pm 50\text{ mm}, z:\pm 50\text{mm}$ $\alpha:\pm 5^\circ, \beta:\pm 5^\circ, \gamma:\pm 5^\circ$

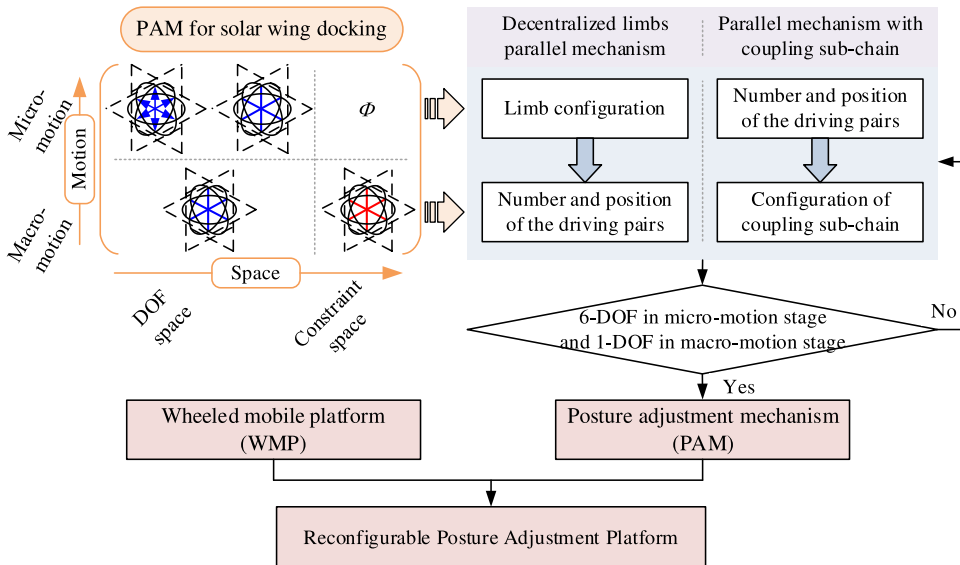


Figure 3. The flowchart of the design method for the RrPAP.

sub-chain between limbs. Among them, the configuration design of traditional PM has been relatively mature, and this paper focuses on the design of the other two configurations.

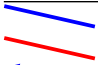
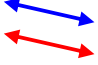
According to the requirements of the docking process, such as DOF and working range, the design index of dual-mode RrPAP can be determined, as shown in Table I.

For the PAM, due to the exchange of moving and fixed platforms in the macro-motion and micro-motion stages, the design process for the configuration of the DLPM is as follows: (1) Based on the DOFs of the PAM in the micro-motion stage, determine the limb configuration. (2) Based on the DOFs of the PAM in the macro-motion stage, determine the number and positions of the driving pairs.

In contrast, the design process for the configuration of the PAM with coupling sub-chains between limbs is as follows: (1) Based on the DOFs and structural symmetry of the PAM in the micro-motion state, determine the number and positions of the driving pairs. (2) Based on the DOFs of the PAM and the number and position of driving pairs in the macro-motion stage, determine the configuration of the coupling sub-chain.

The flowchart of the design method for the RrPAP is shown in Fig. 3. In Fig. 3, the DOF space of PAM with dual motion modes is expressed by line geometry graphical. Using the generalized blending rule, the dual graph of the DOF space of PAM is derived as the constraint space. As shown in Table II, the line and couple vector are denoted by solid line and solid line with double arrows, respectively. The constraint and DOF lines are denoted by blue and red, respectively.

Table II. Basic elements in a line pattern and their meanings.

Basic elements in a line pattern	Mathematical meaning	Physical meaning
	Line vector	Rotational DOF Force constraint
	Couple vector	Translational DOF Couple constraint

3.1. Decentralized limbs parallel mechanism (DLPM)

In the macro-motion stage, the limbs of the DLPM are independent. The ends of n limbs are separated from the ground; they can be regarded as n generalized moving platforms. The vehicle body connecting the decentralized limbs can be regarded as a generalized fixed platform. Each limb must always maintain a particular position, which can be regarded as a serial mechanism in which the prismatic joints are all active driving pairs.

In the micro-motion stage, the ends of n limbs are in contact with the ground, and n contact points form a virtual fixed platform having invariant geometric parameters with the ground. At this time, the vehicle body connecting the decentralized limbs is a moving platform, and its DOF should be six according to the solar wing docking requirements.

3.1.1. The kinematic pairs composition and connection sequence

(i) Limb configuration

In Fig. 3, the base twist screw system of the limb DOF space in the micro-motion stage can be denoted by $\$1 - \6 , which is a six-dimensional twist screw system in the Cartesian coordinate system. $\$1 - \3 denote rotational motion around the three coordinate axes, and $\$4 - \6 denote translational motion along the three coordinate axes.

The twist screw system of different kinematic pairs can be obtained by performing linear combinations of $\$1 - \6 . The limb configuration can be classified according to the number of prismatic joints (PN). This paper explores limb configurations with 6-DOF under conditions where limbs have 0, 1, 2, or 3 prismatic joints. Consequently, the limb configurations are shown in Table III.

In Table III, elements in the limb configuration are represented from left to right as follows: the joints connected to the fixed platform, intermediate joints, and the joints connected to the moving platform.

To simplify the limb configurations, there are three equivalence replacement rules as follows:

- (1) When three revolute joints (R-joints) are mutually perpendicular, the three R-joints can be combined into a spherical joint (S-joint), as shown in Fig. 4(a).
- (2) When two revolute joints are mutually perpendicular, the two R-joints can be combined into a universal joint (U-joint), as shown in Fig. 4(b).
- (3) When a prismatic joint (P-joint) is parallel to a revolute joint, the P-joint and the R-joint can be combined into a cylindrical joint (C-joint), as shown in Fig. 4(c).

The first equivalence replacement rule has been applied in Table III to simplify the three mutually perpendicular revolute joints (R-joints) into a spherical joint (S-joint). In addition, rules two and three can further simplify the configurations of kinematic pairs that satisfy the conditions in Table III. The specific cases are as follows:

- (1) Limb with zero prismatic joints:

Apart from the S-joint, the limb still has three R-joints. When two R-joints are mutually perpendicular, the limb configuration can be simplified into a combination of S, U, and R joints.

Table III. Limb configurations.

Number of the prismatic joint	Twist screw system of limb	Limb configurations
0	$\$_{01} = \$_1 + e_1\$_5 + f_1\$_6,$ $\$_{02} = \$_2 + d_2\$_4 + f_2\$_6,$ $\$_{03} = \$_3 + d_3\$_4 + e_3\$_5,$ $\$_{04} = \$_1 + e_4\$_5 + f_4\$_6,$ $\$_{05} = \$_2 + d_5\$_4 + f_5\$_6,$ $\$_{06} = \$_3 + d_6\$_4 + e_6\$_5$	$SR_1R_2R_3$ $R_1SR_2R_3$ $R_1R_2SR_3$ $R_1R_2R_3S$
1	$\$_{11} = \$_{01}, \$_{12} = \$_{02}, \$_{13} = \$_{03},$ $\$_{14} = d_4\$_4 + e_4\$_5 + f_4\$_6,$ $\$_{15} = \$_{05}, \$_{16} = \$_{06}$	$SP_1R_2R_3$ $SR_1P_2R_3$ $SR_1R_2P_3$ $P_1SR_2R_3$ $R_1SP_2R_3$ $R_1SR_2P_3$ $P_1R_2SR_3$ $R_1P_2SR_3$ $R_1R_2SP_3$ $P_1R_2R_3S$ $R_1P_2R_3S$ $R_1R_2P_3S$ $SP_1P_2R_3$ $SP_1R_2P_3$ $SR_1P_2P_3$ $P_1SP_2R_3$ $P_1SR_2P_3$ $R_1SP_2P_3$
2	$\$_{21} = \$_{01}, \$_{22} = \$_{02}, \$_{23} = \$_{03}, \$_{24} = \$_{14},$ $\$_{25} = d_5\$_4 + e_5\$_5 + f_5\$_6,$ $\$_{26} = \$_{06}$	$P_1R_2SR_3$ $P_1R_2SP_3$ $R_1P_2SP_3$ $P_1P_2R_3S$ $P_1R_2P_3S$ $R_1P_2P_3S$
3	$\$_{31} = \$_{01}, \$_{32} = \$_{02}, \$_{33} = \$_{03}, \$_{34} = \$_{14}, \$_{35} = \$_{25},$ $\$_{36} = d_6\$_4 + e_6\$_5 + f_6\$_6$	$SP_1P_2P_3$ $P_1SP_2P_3$ $P_1P_2SP_3$ $P_1P_2P_3S$

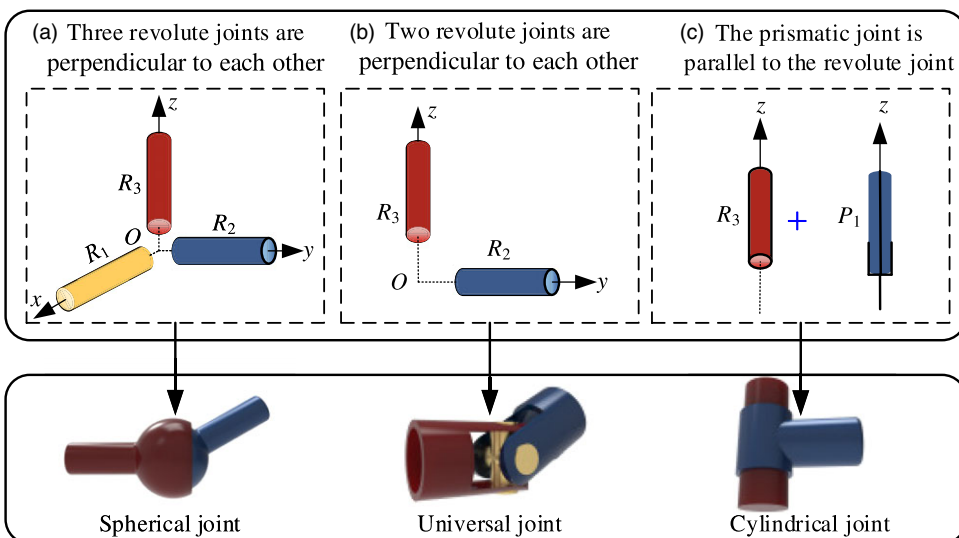


Figure 4. Equivalent replacement rules.

(2) Limb with one prismatic joint:

Apart from the S-joint, the limb has two R-joints and one P-joint. When two R-joints are mutually perpendicular, the limb can be simplified into a combination of S, U, and P joints. When the R-joint is parallel to one of the R-joints, the limb is simplified into a combination of S, C, and R joints.

Table IV. Simplified configurations of limbs.

Type	Number of the prismatic joint	Limb configurations
I	0	SRU SUR RSU USR URS RUS
II	1	SPU SCR SUP SRC PSU RSC CSR USP CRS PUS UPS RCS
III	2	III.1 SPC SCP PSC CSP PCS CPS III.2 R ₁ SP ₂ P ₃ P ₁ P ₂ SR ₃
IV	3	SP ₁ P ₂ P ₃ P ₁ SP ₂ P ₃ P ₁ P ₂ SP ₃ P ₁ P ₂ P ₃ S

(3) Limb with two prismatic joints:

Apart from the S-joint, the limb has one R-joint and two P-joints. When the R-joint is parallel to one of the P-joints, the limb can be simplified into a combination of S, C, and P joints.

The simplified configurations of limbs are shown in Table IV.

(ii) Configuration selection

As shown in Table IV, 30 types of 6-DOF limb configurations are generated in this paper. The characteristics of different configuration limbs are distinct [36–38], and scholars have adopted various methods to select a reasonable limb configuration. In this paper, the selection is based on the functional requirements for PAMs. Since the PAM should weigh 10 tons, the limb configuration is selected based on the mechanism’s load-bearing capacity.

A mathematical model between the non-RPM’s topological structure and structural parameters is established in the paper, which can be denoted as:

$$\begin{cases} F = \sum_{i=1}^n q_i \\ LN = m + n \\ n = F - \sum_{i=1}^n (q_i - 1) \\ q_i \leq F \ (i = 1, 2, \dots, n) \\ n \leq F \end{cases} \tag{1}$$

where F is the DOF of PAM, LN is the number of limbs, m is the number of passive limbs, n is the number of active limbs, and q_i is the DN on the limb i .

In Fig. 2, the moving platform of the PAM is connected to limbs through joints. Geometrically, at least three non-coplanar points can determine a plane. Therefore, the moving platform needs at least three limbs for support. Maintaining structural symmetry can satisfy isotropy requirements according to the topological principles of limbs. Therefore, the topological structure of all limbs should be the same to ensure the structural symmetry of PAM. Consequently, using five limbs in a 6-DOF PAM is not advisable. Moreover, the greater the number of limbs (LN) for a determined mechanism size, the smaller the operational space of the PAM, and the more challenging the structural design. In summary, the LN should be considered as one of the selection criteria. This paper will compare the load-bearing capacity of PAMs with three, four, and six limbs.

In mechanical transmission systems, the more kinematic pairs that are involved, the lower the mechanical efficiency due to factors such as friction. Therefore, the number of kinematic pairs (KSN) should also be considered as one of the selection criteria.

In addition, prismatic and revolute joints are commonly used kinematic pairs for actuation. Compared to the revolute joint, the prismatic joint has a larger load-bearing surface, making it more suitable for bearing heavy loads. Therefore, the PN also needs to be considered as a selection criterion.

As a result, the LN and the sum of the KSN, as well as the PN, are adopted as the criteria for selecting configuration in this paper, as shown in Fig. 5(a)(b). In Fig. 5(a)(b), it can be seen that the more LN there

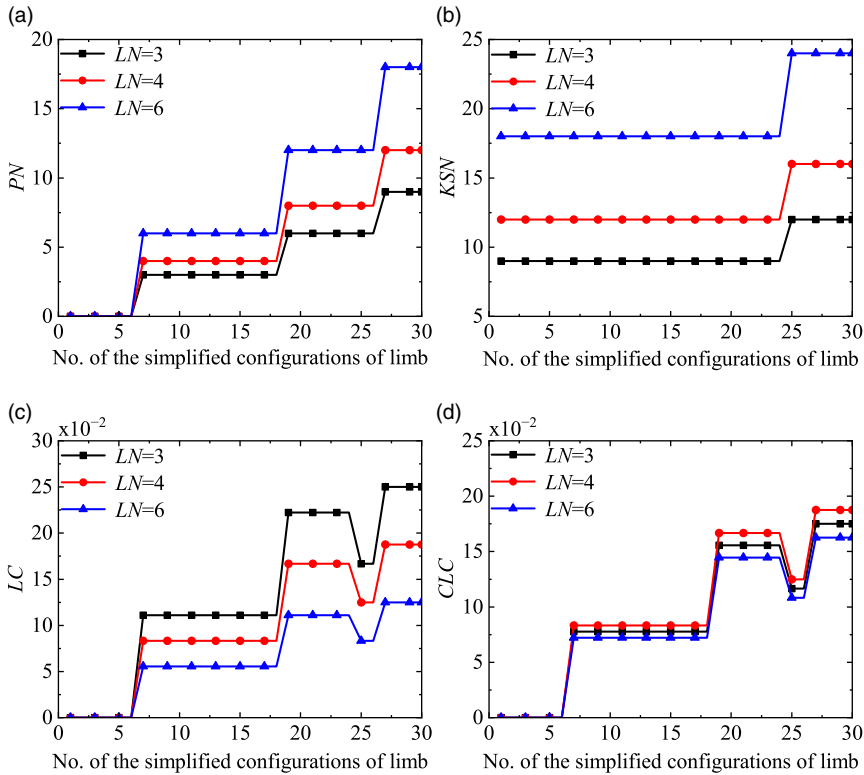


Figure 5. Configuration selection.

is, the larger both PN and KSN are. The expression for each criterion is as follows:

LN = the number of the limbs

$$KSN = i \times LN \tag{2}$$

$$PN = \sum_{j=1}^{LN} P_j$$

where

$$i = \begin{cases} 3 & \text{I, II, III.1} \\ 4 & \text{III.2, IV} \end{cases}, j = 3, 4, 6$$

However, LN, PN, and KSN are not as good as more for the load-bearing capability of PAM. The configuration of the PAM cannot be precisely selected based on the three criteria mentioned above alone. Therefore, the load-bearing capability is defined as:

$$LC = \frac{PN}{LN \times KSN} \tag{3}$$

The comprehensive load-bearing capability is defined as:

$$CLC = k \times \frac{PN}{LN \times KSN} \tag{4}$$

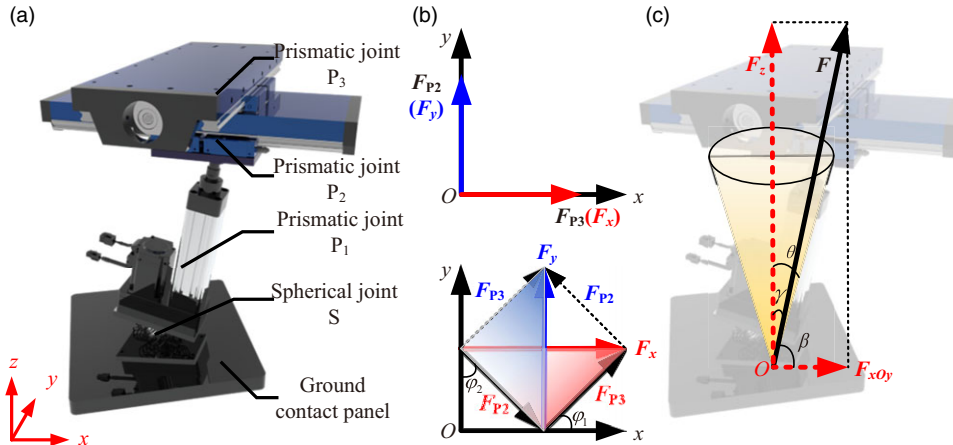


Figure 6. Schematic diagram of force increase in horizontal direction.

where

$$k = \begin{cases} 0.73 - \text{limb PAM} \\ 14 - \text{limb PAM} \\ 1.36 - \text{limb PAM} \end{cases}$$

The coefficient k is determined by factors such as load, motor power, motor volume, overall volume of the mechanism, and so on.

The load-bearing capability and comprehensive load-bearing capability of the limb are shown in Fig. 5(c)(d). In Fig. 5(c), it can be seen that among the limbs with the same LN, those with three prismatic joints, such as SPPP, PSPP, PPS, and PPPS, have better load-bearing capacity. In Fig. 5(d), it can be seen that among PAMs with the same limb configuration, those with four limbs have stronger comprehensive load-bearing capacity. Therefore, for the functional requirements of this paper, suitable decentralized parallel limb configurations are 4-SPPP, 4-PSPP, 4-PPS, and 4-PPPS.

When the 6-DOF PAM is subjected to a load, the limbs will carry a large additional moment in the posture adjustment process, which may impact structural safety and reliability. From the mechanical performance perspective, passive kinematic pairs like spherical joints (S) should be connected to the fixed platform or the moving platform of the PAM to free one end of the limb, preventing it from bearing a substantial bending moment. In conclusion, the 4-SPPP is chosen as the subject of this paper.

(iii) The connection sequence and layout of kinematic pairs

In the layout of horizontal prismatic joints, this paper sets the direction of the second prismatic joint P_2 and the third prismatic joint P_3 of each limb perpendicular to each other and parallel to the upper platform, as shown in Fig. 6(a). They also form a 45° angle with both the first principal motion direction (such as the x -axis) and the second principal motion direction (such as the y -axis), defined as φ_1, φ_2 , as shown in Fig. 6(b). When P_2 and P_3 serve as active joints, according to the principle of force composition, the horizontal driving force can be denoted as:

$$F_x = F_y = \sqrt{F_{P_2}^2 + F_{P_3}^2} \tag{5}$$

When $F_{P_2} = F_{P_3}$, there is $F_x = F_y = \sqrt{2}F_{P_2} = \sqrt{2}F_{P_3}$.

When $F_{P_2} \neq F_{P_3}$, there is $F_x \geq F_{P_2}, F_x \geq F_{P_3}, F_y \geq F_{P_2}, F_y \geq F_{P_3}$.

From Fig. 6(b) and Eq. (6), it can be seen that this layout of horizontal prismatic joints can increase the horizontal driving force without increasing the individual driving force in the horizontal direction.

Let the angle between the first prismatic joint P_1 of each limb in the initial posture and the footpad be β ($\beta < 90^\circ$), as shown in Fig. 6(c), where θ denotes the friction angle. In this paper, if $\beta = 85^\circ$, then

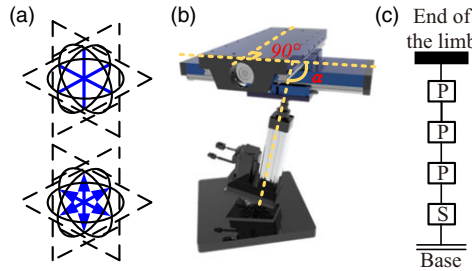


Figure 7. Decentralized limb DOF space and structure.

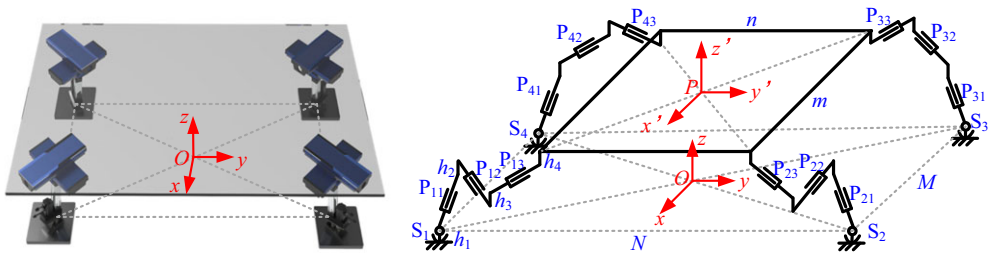


Figure 8. The structure of DLPM.

$\gamma = 5^\circ$. According to reference [39], it is known that $\theta \approx 8 - 10^\circ$ when the footpad is made of rubber. Therefore, $\gamma < \theta$, satisfying the self-locking condition where no matter how heavy the load is, there will be no sliding on the floor.

According to Fig. 6(c), when the first prismatic joint P_1 serves as an active joint, it not only provides a vertical driving force but also a horizontal driving force, which can be denoted as:

$$F_{xoy} = F_{P_1} \cos \beta \tag{6}$$

In conclusion, in order to provide the greater driving force in the horizontal principal motion direction under limited actuation, the DOF space and kinematic pairs layout of the decentralized limb of PAM as shown in Fig. 7, where $\alpha = 95^\circ$. The structure of the DLPM is shown in Fig. 8.

3.1.2. Number and position of driving pairs

If there are passive kinematic pairs of the limbs, the ends of decentralized limbs will exhibit random motion in the macro-motion stage. Consequently, the footpad’s position would not be the same during each landing, leading to the non-uniqueness of the upper platform posture during mode transitions. For the DLPM, it is necessary to ensure that the translational DOF is zero in the macro-motion stage. Then, the DN should satisfy the following condition:

$$DN = PN \times LN \tag{7}$$

The configuration of the DLPM in this paper is 4-SPPP, with three prismatic joints per limb and four limbs. Therefore, the required DN is 12. However, the more driving pairs there are, the greater the difficulty in control [40], so the driving approach is unsuitable.

3.2. Parallel mechanism design with coupling sub-chains between limbs

In order to reduce the DN and further decrease control difficulty, the coupling sub-chains can be formed by designing kinematic pairs between the aforementioned decentralized limbs of the PAM to limit DOF and increase constraints. Therefore, the PAM of PM with coupling sub-chains between the limbs will

be designed in this paper. In this configuration, the limbs of the PAM remain independent and possess multiple DOFs. However, due to coupling sub-chains between limbs, the DOF of the moving platform is not determined by the common DOF of the limbs but rather related to the structure of the coupling sub-chains between limbs.

In the macro-motion stage, the ends of the n limbs are separated from the ground. The vehicle body connecting the decentralized limbs can be considered a generalized fixed platform. The ends of the n limbs are connected through coupling sub-chains between limbs, forming a generalized moving platform.

In the micro-motion stage, the ends of the n limbs are in contact with the ground. The coupling sub-chains between limbs lose their effect, resulting in a reduction in the effective links. At this time, similar to the DLPM, the n contact points with the ground form a virtual fixed platform with invariant geometric parameters. The vehicle body connecting the limbs becomes the moving platform.

3.2.1. Number and position of driving pairs

The 4-SPPP mechanism has 6-DOF, so theoretically, only six inputs are needed. In this paper, the selection rules for the DN are as follows to meet the functional requirements:

- (1) Redundant drives can be used to avoid singular configurations.
- (2) To achieve structural symmetry in design, the DN for four-limb PAM should be a multiple of four, that is $DN = 4i (i = 1, 2, \dots)$ and $DN \leq PN \times LN$.

Therefore, this paper selects eight driving pairs for the next design. In order to ensure load-bearing capacity in the vertical direction, driving motors are assigned to the first prismatic joints of all four limbs. Simultaneously, to avoid generating additional torques, the arrangement of the four horizontal drives should be in the same plane. From Fig. 6, it can be seen that the second prismatic joint and the third prismatic joint of each limb have the same effect as the active drive. Therefore, the second prismatic joints of the four limbs are selected as the driving pair in this paper.

3.2.2. Reconfigurable mechanism design

The type synthesis of a reconfigurable mechanism is the reverse process of state change. In the transformation process from the initial state (macro-motion) to the final state (micro-motion), the number of effective links in a reconfigurable mechanism generally decreases, leading to changes in the DOF. The type synthesis of a reconfigurable mechanism is based on the topological structure of the final state (micro-motion), that is, the DLPM designed above. By adding series-coupled kinematic pairs, the translational DOFs of the moving platform are further constrained to finally obtain the initial state (macro-motion) configuration.

In this paper, a coupled mechanism model with multi-loop consists of serial coupling sub-chains is formed by adding series coupling sub-chains between decentralized limbs as shown in Fig. 9. Figure 9(a) illustrates the topology of the PM with coupling sub-chains between limbs, and Fig. 9(b) shows the planar topological structure with coupling sub-chains. In macro-motion mode, any footpad, such as link i , link j , or link k , can serve as an independent moving platform.

To ensure that all four footpads can have the same DOF when functioning as the moving platform, the coupled mechanism should possess the following characteristics:

- (1) Limb 2 + Coupling sub – chain 5 = Limb 3 + Coupling sub – chain 7, from Limb 2 = Limb 3, it follows that Coupling sub – chain 5 = Coupling sub – chain 7.
- (2) Coupling sub-chain is equal to shared sub-chain, that is, Coupling sub – chain 6 = Coupling sub – chain 8.

From this, it can be inferred that the dual-mode PAM with coupling sub-chains between limbs is a symmetrical coupled mechanism. The flowchart of the configuration synthesis process is shown in Fig. 10.

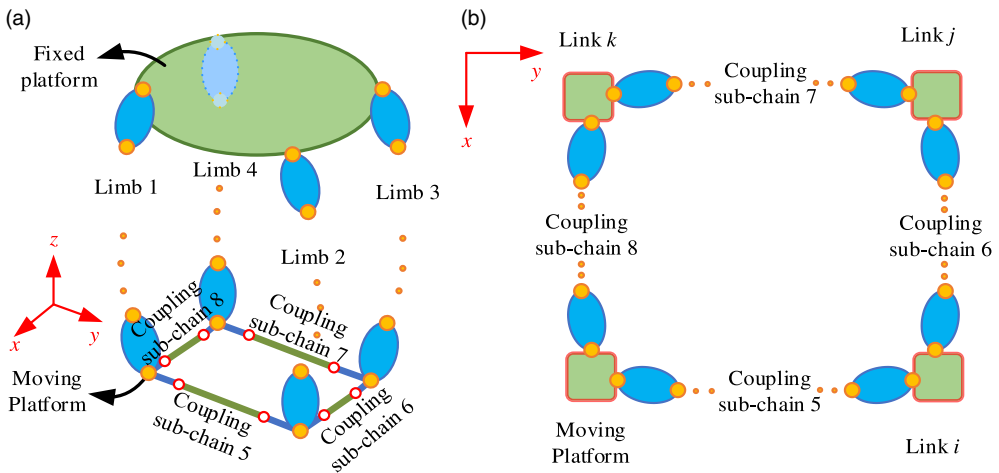


Figure 9. Coupled mechanism model with multi-loop consists of serial coupling sub-chains.

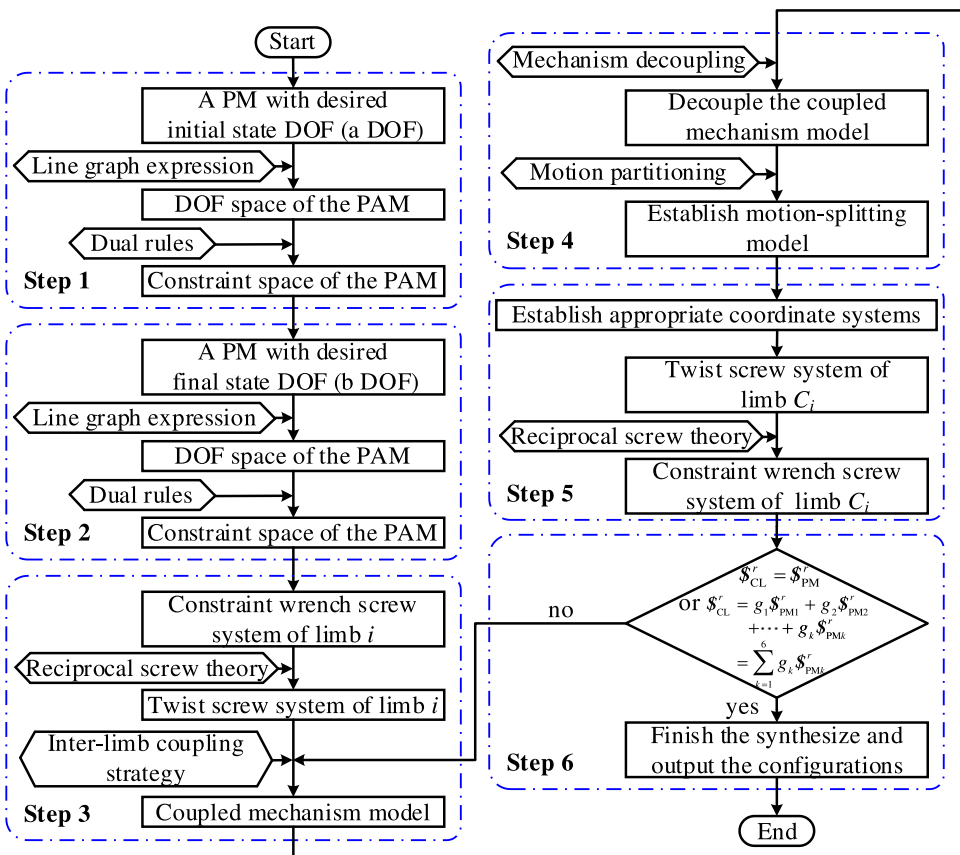


Figure 10. The flowchart of configuration synthesis process of symmetrical coupled mechanism.

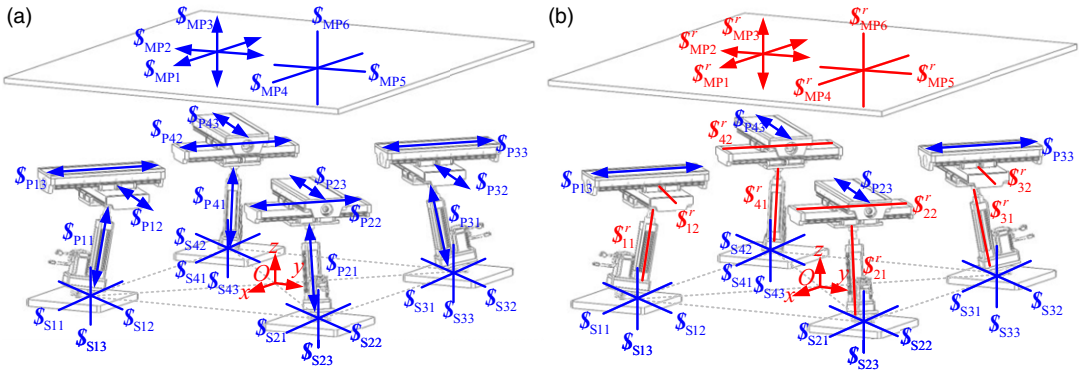


Figure 11. The constraint wrench analysis of decentralized limbs PAM.

The detailed steps for configuration synthesis are as follows:

Step 1: Select a PM with the desired final state DOF (a -DOF). Analyze the motion and constraint properties of the PM based on screw theory.

Step 2: Analyze the twist screw system \mathcal{S}_{PMi} of the mechanism with the desired initial state DOF (b -DOF). Using reciprocal screw theory, the constraint wrench screw system \mathcal{S}_{PM}^r or the basic constraint wrench screw system \mathcal{S}_{PMi}^r of the initial state mechanism can be obtained.

Step 3: Construct a coupled mechanism model with multi-loop consists of serial coupling sub-chains. Analyze the motion properties \mathcal{S}_{Li} of each limb and then add the appropriate serial coupling sub-chain (coupling sub-chain i) between Limb m and Limb n .

Step 4: Decouple the coupled mechanism model and establish a motion-splitting model using the motion partitioning method. Divide the basic model into $2LN-1$ individual limbs, which are denoted by Limb Ci .

Step 5: Under the initial configuration, take Limb Ci as the research object. Based on screw theory, analyze the motion and constraint properties of Limb Ci . Establish appropriate coordinate systems, and the twist screw system \mathcal{S}_{CLi} of Limb Ci can be determined. Using reciprocal screw theory, the constraint wrench screw system \mathcal{S}_{CLi}^r of Limb Ci can be obtained.

Step 6: Confirming the correctness of the PM structure with coupled limbs can be done through two methods:

a. Check if the union of constraint wrench screw systems \mathcal{S}_{CL}^r of coupled limbs is equal to the expected constraint wrench screw system \mathcal{S}_{PM}^r , that is, $\mathcal{S}_{CL}^r = \mathcal{S}_{PM}^r$.

b. Check if the union of constraint wrench screw systems \mathcal{S}_{CL}^r of coupled limbs can be linearly combined from the expected basic constraint wrench screw system \mathcal{S}_{PMi}^r , that is, $\mathcal{S}_{CL}^r = g_1\mathcal{S}_{PM1}^r + g_2\mathcal{S}_{PM2}^r + \dots + g_k\mathcal{S}_{PMk}^r = \sum_{k=1}^6 g_k\mathcal{S}_{PMk}^r$, where g_k is the linear combination coefficient, when $\mathcal{S}_{PMk}^r = 0$, it follows that $g_k = 0$.

The analysis process of this article is as follows:

Step 1: The 4-SPPP 3T3R symmetrical PAM with 6-DOF based on the decentralized limb configuration mentioned above is selected to study in this paper. The motion and constraint properties of the PAM are analyzed based on screw theory.

Establish the coordinate system O_{xyz} ; the coordinate origin O is the connection point of the four S-joint centers. The x -axis points from S-joint 4 to S-joint 1, the y -axis points from S-joint 4 to S-joint 3, and the z -axis is determined by the right-hand rule, as shown in Fig. 11. In the final state, the moving platform is the upper platform. Figure 11(a) shows the constraint wrench analysis of the PM with decentralized limbs. Based on the number and positions of the driving pairs determined in the previous section, lock the active driving pairs, and the constraint wrench analysis is shown in Fig. 11(b).

Step 2: This paper focuses on ground adaptability in micro-motion mode, with an expected DOF for the footpad being 2R or 1R. Taking 1R as an example, analyze the twist screw system $\$_{PMi}^r$ of the mechanism with 1R DOF. Using reciprocal screw theory, the basic constraint wrench screw system $\$_{PMi}^r$ of the initial state mechanism can be obtained.

To ensure that the limb landing points remain at the same position during mode transition, the target basic constraint wrench screw system at the center S_i of the spherical joint should be as follows:

$$\begin{aligned} \$_{si1}^r &= (1, 0, 0; 0, 0, 0) \\ \$_{si2}^r &= (0, 1, 0; 0, 0, 0) \\ \$_{si3}^r &= (0, 0, 1; 0, 0, 0) \end{aligned} \tag{8}$$

According to the reciprocity of the screw, the basic twist screw system at point S_i can be obtained as:

$$\begin{aligned} \$_{si1} &= (1, 0, 0; 0, 0, 0) \\ \$_{si2} &= (0, 1, 0; 0, 0, 0) \\ \$_{si3} &= (0, 0, 1; 0, 0, 0) \end{aligned} \tag{9}$$

where $\$_{si3}$ does not affect the ground adaptation requirements of the mechanism and can be considered a local DOF. Additionally, $\$_{si3}$ would lead to the generation of movement within the xy plane for the DLPM, which means that it cannot constrain the motion of the passive pairs in macro-motion stage. Therefore, it should be discarded.

In the initial state, the moving platform contacts the ground through various footpads. Therefore, the footpads possess a basic twist screw system with 1R DOF, which is given by:

$$\$_{PM1} = (1, 0, 0; 0, 0, 0) \text{ or } \$_{PM2} = (0, 1, 0; 0, 0, 0) \tag{10}$$

Then, the basic constraint wrench screw system of the footpads is:

$$\begin{aligned} \$_{PM1}^r &= (1, 0, 0; 0, 0, 0) & \$_{PM1}^r &= (1, 0, 0; 0, 0, 0) \\ \$_{PM2}^r &= (0, 1, 0; 0, 0, 0) & \$_{PM2}^r &= (0, 1, 0; 0, 0, 0) \\ \$_{PM3}^r &= (0, 0, 1; 0, 0, 0) \text{ or } \$_{PM3}^r &= (0, 0, 1; 0, 0, 0) \\ \$_{PM4}^r &= (0, 0, 0; 0, 1, 0) & \$_{PM4}^r &= (0, 0, 0; 1, 0, 0) \\ \$_{PM5}^r &= (0, 0, 0; 0, 0, 1) & \$_{PM5}^r &= (0, 0, 0; 0, 0, 1) \end{aligned} \tag{11}$$

Step 3: Construct a coupled mechanism model with primary nodes, analyze the twist screw system $\$_{Li}$ of each limb, and then add serial coupling sub-chain (Coupling sub-chain 5) between the decentralized limbs Limb 1 and Limb 2, similarly, add Coupling sub-chain 6 between Limb 2 and Limb 3, Coupling sub-chain 7 between Limb 3 and Limb 4, and Coupling sub-chain 8 between Limb 4 and Limb 1, as shown in Fig. 9.

This paper considers the serial coupling sub-chain without drivers and forced to undergo determined motion as passive constraint limbs. Their primary function is to constrain one or several DOFs of the moving platform to achieve the expected motion. In addition, constraint limbs can also improve the stiffness of the mechanism.

The constraint wrench screw systems of limbs are the same as the constraint wrench screw systems of mechanism. Therefore, the standard basis for the initial state limb twist screw system can be obtained as follows:

$$\begin{aligned} \$_{L1} &= \$_{PM1} = (1, 0, 0; 0, 0, 0) \\ \$_{L2} &= \$_{PM2} = (0, 1, 0; 0, 0, 0) \end{aligned} \tag{12}$$

where $\$_{i1}$ and $\$_{i2}$ are the mechanism constraint wrench line vectors along the x and y directions, respectively, intersecting at the origin of the reference coordinate system, can be generated in various forms of limb motion limbs through linear combinations and different arrangements of two twist screw systems.

Table V. Hinge arrangement and combination of kinematic pairs in serial constraint limbs.

DOF	Arrangement mode	Geometric constraints	Combination mode
1	RR*	The two rotating shafts of RR* coincide	4R 4RR* 4RR^4U 4RU 4UU2(RR*-RU) 2(RR*-U)
2	RR^ U RU	The two rotating shafts of RR^ coincide The rotating shaft of R coincides with one of the rotating shafts of U	2(RR*-UU)1RR*-3RU 1RR*-3U 1RR*-3UU3RR*-1RU 3RR*-1U 3RR*-1UU2(U-RU) 2(U-UU) 1U-3RU1U-3UU 3U-1RU
3	UU	One of the U shafts coincides with another U shaft	3U-1UU2(RU-UU) 1RU-3UU 3RU-1UU

Note^a: RR* is equivalent to R. When the four coupling sub-chains are not completely identical, in order to satisfy the symmetry of the mechanism, both R and RR* are represented as RR*.

Note^b: RR^ is equivalent to U. When the four coupling sub-chains are not completely identical, for simplicity of expression, both RR^ and U are represented as U.

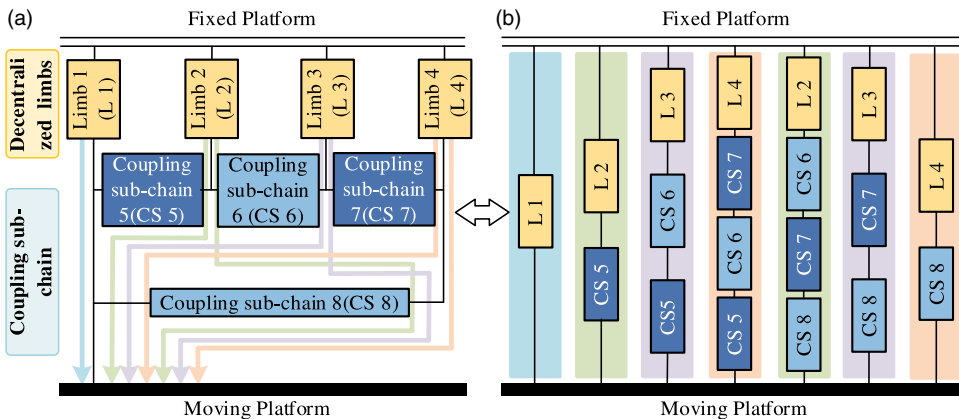


Figure 12. Motion distribution model of coupled mechanism.

The general expression of a kinematic pair is:

$$\mathcal{L}_i = a\mathcal{L}_{L1} + b\mathcal{L}_{L2} = (a, b, 0; 0, 0, 0) \tag{13}$$

where a and b are not both 0, they can form a 2R limb that rotates in the x and y directions.

When the kinematic pair refers to a rotating joint, it is evident that $a^2 + b^2 = 1$.

According to the limb comprehensive method, the direction of the rotational axis of the revolute joint can be arbitrary. The rotational axis of the revolute joint is perpendicular to the constraint force. By analyzing the standard basic twist screw system, it can be inferred that the rotation axis for the revolute joint can be in any direction within the xy plane. Therefore, it can be inferred that there will be R_x , R_y , and U_{xy} in the limb. In this paper, R_x and R_y denote a revolute joint with the x -axis and y -axis as the rotational axis, respectively, and U_{xy} denotes joints with rotational axes in the x and y directions. As a result, the arrangement and combination of kinematic pairs in serial constraint limbs are presented in Table V.

Due to the functional requirements of this paper, it is necessary for the four coupling sub-chains to have opposite sides pairwise identical. Therefore, the available combinations for serial coupling sub-chain in this paper include 4R, 4RR*, 4RR^, 4U, 4RU, 4UU, 2(RR*-RU), 2(RR*-U), 2(RR*-UU), 2(U-RU), 2(U-UU), and 2(RU-UU).

Step 4: According to Fig. 12(a), the coupled mechanism model is decoupled into seven individual limbs, as shown in Fig. 12(b).

Among them, Limb 1 is one limb of the original DLPM, Limb 2→Limb 5, Limb 3→Limb 6→Limb 5, Limb 4→Limb 7→Limb 6→Limb 5, Limb 2→Limb 6→Limb 7→Limb 8, Limb 3→Limb 7→Limb 8, and Limb 4→Limb 8 are six coupled limbs containing serial coupling sub-chains. The decoupled limbs are denoted as Limb C_i ($i = 1-7$), from left to right, labeled as Limb C1 to Limb C7.

Step 5: In the initial configuration, taking the individual limb (Limb C_i) containing serial coupling sub-chain as the research object, based on screw theory, analyze the motion and constraint of the decoupled coupled limbs in the coupled mechanism. Utilizing the coordinate system construction method shown in Fig. 11(b), the twist screw system $\$_{CL_i}$ of Limb C_i is determined. Using reciprocal screw theory, the constraint wrench screw system $\$_{CL_i}^r$ of Limb C_i can be obtained.

Taking 2(RR*-UU) as an example for illustration in this paper. Let Limb 5 = Limb 7 = UU and Limb 6 = Limb 8 = RR*. In the coupling sub-chain, the two rotation axes of RR* are coaxial, which can be integrated into a single R. Taking Limb C3 as an example, composed of Limb 3, Limb 6, and Limb 5, where the twist screw system of Limb 3 is:

$$\begin{aligned}
 \$_{L31} &= (0, 0, 0; -d, e, 0) \\
 \$_{L32} &= (1, 0, 0; 0, 0, -b) \\
 \$_{L33} &= (0, 1, 0; 0, 0, -a) \\
 \$_{L34} &= (0, 0, 1; b, a, 0)
 \end{aligned}
 \tag{14}$$

The twist screw system of Limb 6 is:

$$\$_{L6} = (1, 0, 0; 0, l_1, -n_1)
 \tag{15}$$

The twist screw system of Limb 5 is:

$$\begin{aligned}
 \$_{L51} &= (1, 0, 0; 0, l_2, -n_2) \\
 \$_{L52} &= (1, 0, 0; 0, l_2, n_2) \\
 \$_{L53} &= (0, 1, 0; -l_2, 0, m_2)
 \end{aligned}
 \tag{16}$$

Then, the twist screw system of Limb C3 is:

$$\begin{aligned}
 \$_{CL31} &= (0, 0, 0; -d, e, 0) \\
 \$_{CL32} &= (1, 0, 0; 0, 0, -b) \\
 \$_{CL33} &= (0, 1, 0; 0, 0, -a) \\
 \$_{CL34} &= (0, 0, 1; b, a, 0) \\
 \$_{CL35} &= (1, 0, 0; 0, l_1, -n_1) \\
 \$_{CL36} &= (1, 0, 0; 0, l_2, -n_2) \\
 \$_{CL37} &= (1, 0, 0; 0, l_2, n_2) \\
 \$_{CL38} &= (0, 1, 0; -l_2, 0, m_2)
 \end{aligned}
 \tag{17}$$

Taking the inverse screw, the constraint wrench screw system of Limb C3 can be derived as:

$$\begin{aligned}
 \$_{CL31}^r &= (0, 0, 1; b, a, 0) & b = n, a = m \\
 \$_{CL32}^r &= (e, d, 0; -dl_1, el_2, be + ad) & l_1 = l_2
 \end{aligned}
 \tag{18}$$

The detailed analysis of the twist/constraint wrench screw systems of the decoupled limbs of the PM with serial coupling sub-chains can be found in Table VII. The union of the constraint wrench screw

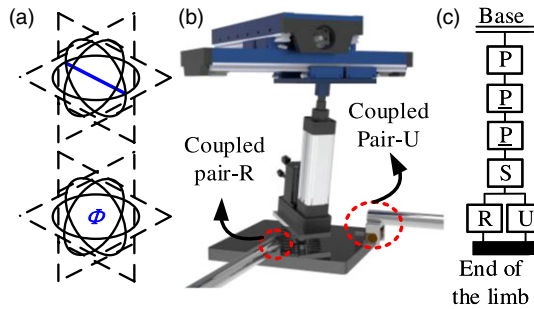


Figure 13. Coupled limb DOF space and structure.

system of each decoupled limb is:

$$\begin{aligned}
 \$_{CL1}^r &= (0, 0, 1; -b, -a, 0) \\
 \$_{CL2}^r &= (e, d, 0; 0, 0, -(be + ad)) \\
 \$_{CL3}^r &= (0, 0, 1; b, -a, 0) \\
 \$_{CL4}^r &= (e, -d, 0; dl_1, el_2, -(be + ad)) \\
 \$_{CL5}^r &= (0, 0, 1; b, a, 0) \\
 \$_{CL6}^r &= (e, d, 0; -dl_1, el_2, -(be + ad)) \\
 \$_{CL7}^r &= (0, 0, 1; -b, a, 0) \\
 \$_{CL8}^r &= (-e, d, 0; -dl_1, -el_2, -(be + ad))
 \end{aligned}
 \tag{19}$$

Step 6: Through analysis, it can be determined that the union of the constraint wrench screw systems of the coupled limbs can be linearly combined to form the desired basic constraint wrench screw system. Therefore, the correctness of the PM structure with coupled limbs can be determined.

The aforementioned union of constraint wrench screw systems for the coupled limbs is indeed the constraint wrench screw system for the moving platform. Thus, it follows that the twist screw system of the footpad is:

$$\$_1 = (1, 0, 0; 0, 0, b)
 \tag{20}$$

In this paper, after introducing the serial coupling sub-chains 2(RR*-UU) between the decentralized limbs, the union of constraint wrench screw systems for the coupled limbs equals the desired constraint wrench screw system. The results show that the moving platform (footpad) has only 1R DOF, and the rotation axis direction for the footpad is determined by the R rotation axis direction. At this point, the translational freedom of the passive pairs can be locked, satisfying the requirement for consistency in the position of the limb ends during mode transition. Similarly, it can be determined that RxUxy-RyUxy-RxUxyRy, RxRx-RyUxy-RxRx-UxyRy/RyRy-RxUxy-RyRy-UxyRx and RxRx-Uxy-RxRx-Uxy/RyRy-Uxy-RyRy-Uxy all satisfy the requirement above.

In summary, to ensure consistency in the position of the limb ends during mode transitions and meet ground adaptation, it is necessary to ensure that the moving platform has 1R or 2R DOF in the macro-motion stage. To achieve this, coupling sub-chains are designed between the limb ends based on DLPM, utilizing multiple coupling kinematic pairs to constrain the translational motion of DLPM. Thus, to satisfy the symmetry requirements in the structure, the four decentralized limbs of DLPM are connected with two sets of RR*-UU in this paper. The DOFs of the mechanism in the macro-motion stage can be satisfied when the common axis of UU and the common axis of RR are perpendicular to each other. Ultimately, the configuration of the PAM is determined as 4-SPPP-2(RR*-UU), and the limb DOF space and structural layout are shown in Fig. 13.

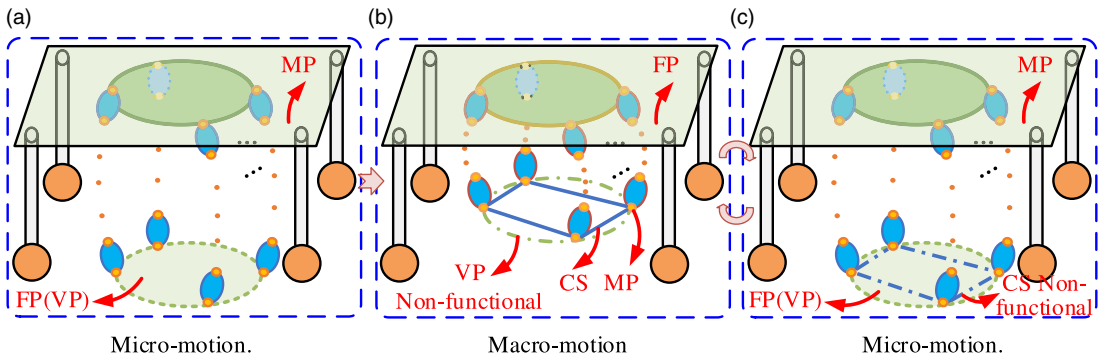


Figure 14. The reconfiguration process of RrPAP. Note: MP denotes the moving platform, and FP denotes the fixed platform, VP denotes the virtual platform, and CS denotes the coupling sub-chain.

4. The realization and analysis of RrPAP

4.1. The realization of RrPAP

In this paper, a decentralized four-limb PAM that can realize (6-DOF) motion in the micro-motion stage is designed. In this stage, the moving platform is the vehicle body, and the fixed platform is the virtual platform formed by the decentralized limbs in contact with the ground, as shown in Fig. 14(a).

In the macro-motion stage, the decentralized limbs are shortened and separated from the ground, the virtual platform is nonfunctional. The PAM operates as an open-loop structure with multiple DOFs. The fixed platform is the vehicle body, and the moving platform is the end of the decentralized limbs. In this stage, the same DN as DOF are required to control the motion. However, the increase of the DN increases the difficulty of the control. In the condition of the reduction of the driving pairs, in order to enable the PAM to have a defined motion after being released from ground constraints, a serial coupling sub-chain is designed between adjacent limbs to restrict relative movement between them, as shown in Fig. 14(b).

The mode transformation is performed again, and in the micro-motion stage, the four limbs of PAM are elongated. The limb establishes a stable connection with the ground, transforming the PAM into a closed-loop structure. Then, the serial coupling sub-chain between adjacent limbs is nonfunctional, as shown in Fig. 14(c).

To summarize, whether the virtual platform or coupling sub-chain is nonfunctional or not depends on whether the decentralized branches of the PAM are in contact with the ground during the mode transformation process; that is, the configurations of the PAM are different in different modes, which enables the reconfiguration function to be realized.

Specifically, the RrPAP proposed in this paper is based on a decentralized n -SPPP topology structure, using two sets of identical RR*-UU chains for coupling, as shown in Fig. 15(a). The joint loop diagram is shown in Fig. 15(b), and the realization of the RrPAP is shown in Fig. 15(c). In summary, the RrPAP for solar wing docking consists of a WMP and a PAM. A four-Mecanum-wheeled omnidirectional mobile system is used for the structure design of the WMP in this paper. The PAM is designed by a 6-DOF PM to fulfill the functional requirement. The design of the 6-DOF PAM involves coupled sub-chains to constrain the DOFs of passive pairs in the macro-motion stage. The configurations of all four limbs are SPPP, and the ends of decentralized limbs are connected in series by mutually perpendicular RR*-UU sub-chains to form the reconfigurable mechanism.

4.2. The motion simulation of RrPAP

From the reconfiguration process of RrPAP in Fig. 14, it can be seen that the moving and fixed platforms of the RrPAP are interchanged during the mode transfer. Therefore, this paper takes the motion of PAM in the micro-motion stage as an example for motion simulation.

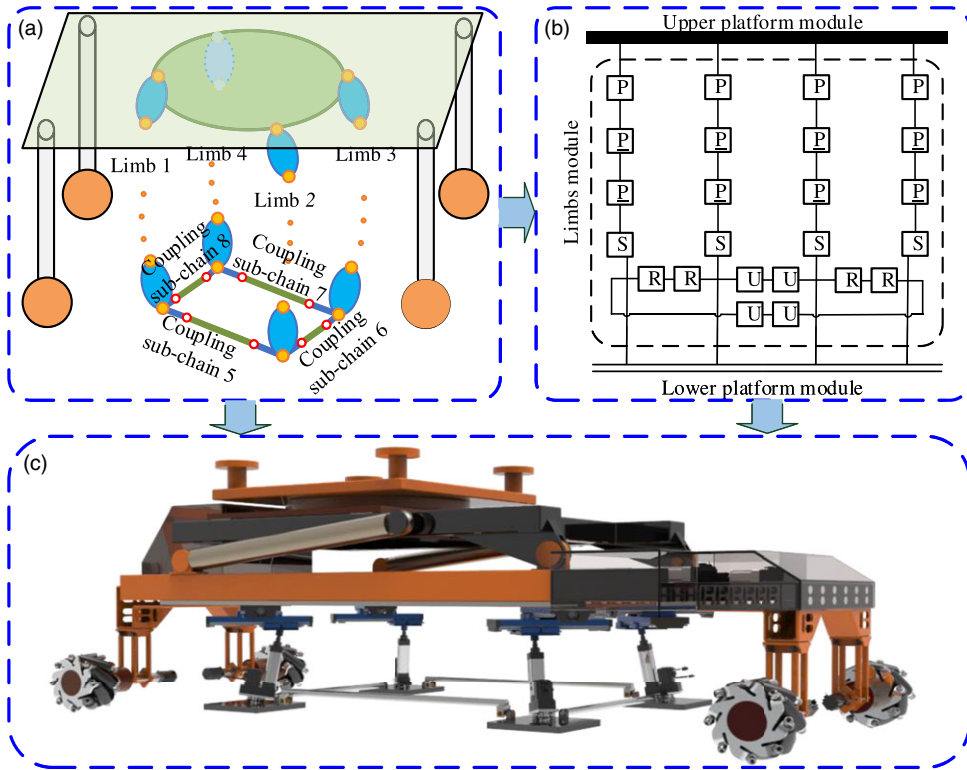


Figure 15. realization of RrPAP for solar wing docking.

4.2.1. Trajectory planning

In the layout of horizontal prismatic joints, this paper sets the direction of the second prismatic joint P_2 . It is assumed that the PAM needs to reach the maximum range of the posture adjustment within 5s, that is, moving 50 mm along the coordinate axis and rotating 5° around the coordinate axis. In order to reduce the impact and inertia force during the movement of the PAM, it is hoped that the movement of the posture process is smooth under the ideal state. Let the displacement, velocity, and acceleration of the moving and rotating of the RrPAP satisfy the following equations:

$$\begin{cases} s_{t=0} = 0 \\ s_{t=5} = 50 \end{cases} \begin{cases} \dot{s}_{t=0} = 0 \\ \dot{s}_{t=5} = 0 \end{cases} \begin{cases} \ddot{s}_{t=0} = 0 \\ \ddot{s}_{t=5} = 0 \end{cases} \quad (21)$$

$$\begin{cases} \theta_{t=0} = 0^\circ \\ \theta_{t=5} = 5^\circ \end{cases} \begin{cases} \dot{\theta}_{t=0} = 0 \\ \dot{\theta}_{t=5} = 0 \end{cases} \begin{cases} \ddot{\theta}_{t=0} = 0 \\ \ddot{\theta}_{t=5} = 0 \end{cases}$$

Hence, the movement driver function can be denoted as:

$$Y = 50 \left(\frac{t}{5} - \frac{1}{2\pi} \sin \frac{2\pi t}{5} \right) (0 \leq t \leq 5) \quad (22)$$

And the rotation driver function can be denoted as:

$$Y = 5 \left(\frac{t}{5} - \frac{1}{2\pi} \sin \frac{2\pi t}{5} \right) (0 \leq t \leq 5) \quad (23)$$

The trajectory is plotted according to the Eqs. (22) and (23), as shown in Fig. 16(a).

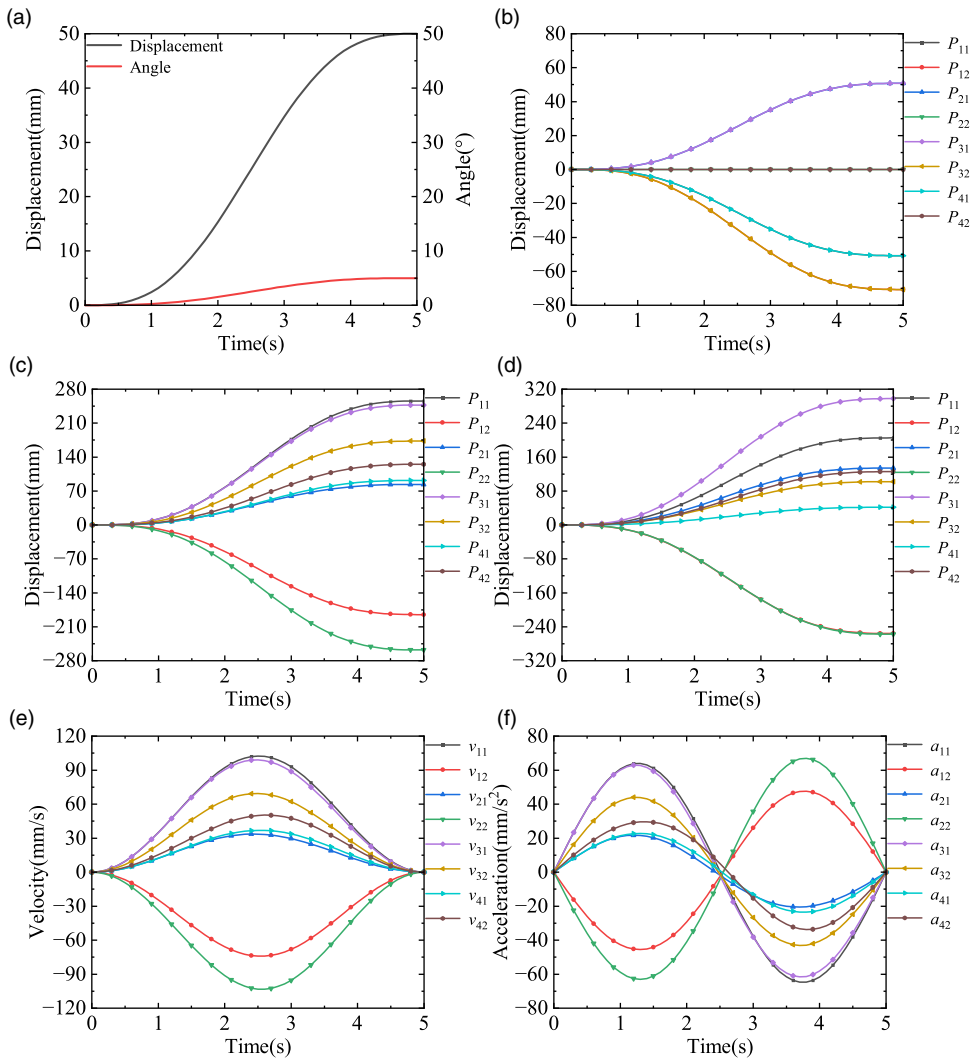


Figure 16. Motion simulation.

4.2.2. Motion simulation

The DOF of PAM is 6, and three typical motion modes, 3T, 3R, and 3T3R, were selected for motion simulation in ADAMMS in this paper. The trajectory equation of the center reference point of the moving platform is determined according to the Eqs. (22) and (23). The main structural parameters of the PAM are shown in Fig. 9, and their values are shown in Table VI.

Figure 16(b)–(d) shows the simulation curves of the relative displacement of the active driving pairs of each limb obtained by ADAMS simulation of the mechanism model in three typical motion modes, respectively. Figure 16(e)–(f) shows the simulation curves of the velocity and acceleration of the active driving pairs of each limb obtained by ADAMS simulation of the mechanism model with 3R motion modes.

4.3. The workspace of RrPAP

Macro-motion is realized by WMP and micro-motion is realized by PAM. Therefore, the workspace of WMP is not restricted by PM, and only the workspace of PAM needs to be analyzed in this paper. In order to verify whether the PAM can meet the design requirements of the micro-motion, the workspace of the PAM is analyzed in this paper.

Table VI. The main structural parameters of the PAM mechanism.

Parameters/unit	Value	Parameters/unit	Value
M/mm	1850	h_1/mm	15
N/mm	3850	h_2/mm	30
m/mm	1750	h_3/mm	45
n/mm	3750	h_4/mm	60

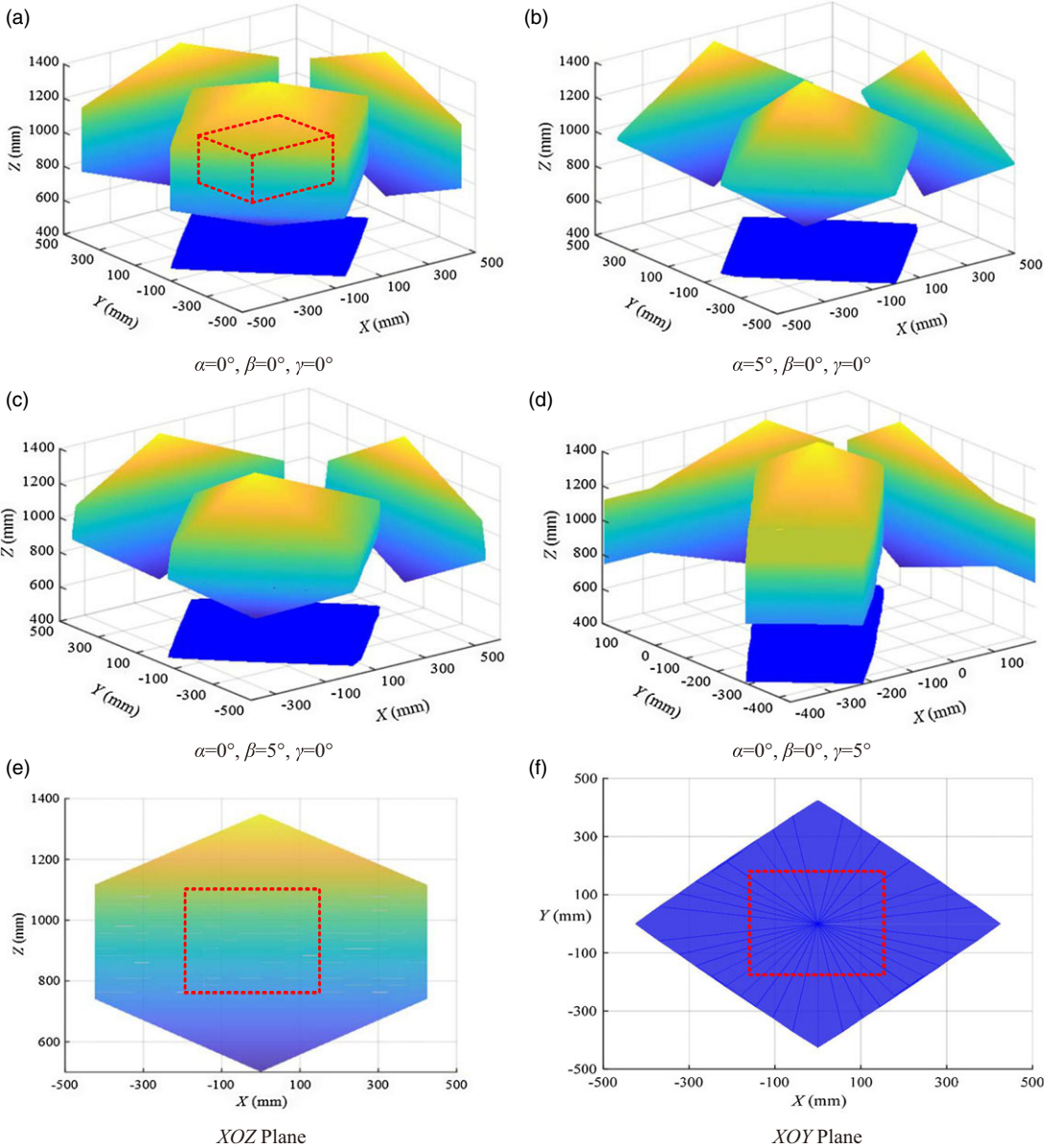


Figure 17. The workspace of PAM.

In this paper, a numerical method of boundary search is used to generate the workspace of PAM by considering the joint angle constraints, actuated joint stroke limitations, and redundantly actuated joint limitations, as shown in Fig. 16. The workspace at the initial posture is shown in Fig. 17(a), and the position workspace for various postures is shown in Fig. 17(b)–(d). It can be seen that the position workspace has different shapes and volumes at diverse postures.

Figure 17 shows that the PAM has a large workspace and good continuity. Taking the workspace at the initial posture as an example, the projections of this workspace onto the XOZ and XOY planes are shown in Fig. 17(e) and Fig. 17(f), respectively. The workspace contains a cube with a length, width, and height of 350 mm, which can meet the requirements of the moving range (± 50 mm) in the micro-motion stage.

5. Conclusion

In order to enable a posture adjustment device to meet the requirements of different-sized satellites docking with solar wings, a movable RrPAP for posture adjustment of the satellite is proposed in this paper, which has two motion modes. The layout of the dual-mode RrPAP is designed. Considering the DOFs of the PAM in the micro-motion stage and the heavy-load requirement, the comprehensive load-bearing index is proposed for configuration selection. The results show that a DLPM with three P joints and four limbs has a stronger load-bearing capacity. The design method of serial coupling sub-chains is proposed to limit the end DOF of the decentralized limb in the macro-motion stage. Four types of symmetrically coupled mechanisms suitable for satellite posture adjustment in the solar wing docking process are derived. Taking 4-SPPP-2(RR*-UU) as an example to verify the feasibility of this design method. This paper provides an important theoretical foundation for designing RrPAP for solar wings. It has broad application prospects in the aerospace field, particularly in the assembly of large-scale components.

Author contributions. Rui Wang, Jinzhu Zhang, and Xiaoyan Xiong conceived and designed the study. Rui Wang wrote the initial draft. Jinzhu Zhang reviewed, commented, and revised the first draft. Ruilin Yuan completed the drawing of the 3D model and visualization of the method.

Acknowledgments. This work is supported by the National Natural Science Foundation of China (Grant No. 51905367).

Competing interests. The authors declare no competing interests exist.

Ethical approval. None.

References

- [1] W. Zhang, S. Lu and X. Ding, "Recent development on innovation design of reconfigurable mechanisms in China," *Front Mech Eng* **14**(1), 15–20 (2019).
- [2] H. Shi, J. Zhang, T. Wang, R. Li and Q. Huang, "Mechanism design and kinematic analysis of a bioinspired 5-DOF parallel driving mechanism," *Mech Mach Theory* **181**, 105178 (2023).
- [3] Y. Huang, J. Zhang and X. Xiong, "Closed-form dynamic modeling and performance evaluation of a 4-degrees-of-freedom parallel driving mechanism," *J Mech Robot* **16**(7), 071012 (2024).
- [4] M. Furqan, M. Suhaib and N. Ahmad, "Studies on Stewart platform manipulator: A review," *J Mech Sci Technol* **31**(9), 4459–4470 (2017).
- [5] L. Z. Zhu, L. P. Wang and J. S. Zhao, "Mechanism Synthesis and Workspace Analysis of a Spraying Robot for Airfoil," **In: 3rd IEEE/IFToMM/ASME International Conference on Reconfigurable Mechanisms and Robots (ReMAR 2015)**, Beijing, China (2015).
- [6] Y. Y. Huang, J. Z. Zhang, X. Y. Xiong and S. X. Liu, "Kinematic and dynamic analysis of a 4-DOF over-constraint parallel driving mechanism with planar sub-closed chains," *Robotica* **41**(10), 3137–3159 (2023).
- [7] M. G. Mohamed and C. M. Gosselin, "Design and analysis of kinematically redundant parallel manipulators with configurable platforms," *IEEE Trans Robot* **21**(3), 277–287 (2005).
- [8] P. Lei and L. Zheng, "An automated in-situ alignment approach for finish machining assembly interfaces of large-scale components," *Robot Comput Integr Manuf* **46**, 130–143 (2017).

- [9] W. Fan, L. Zheng, W. Ji, X. Xu, L. Wang, Y. Lu and X. Zhao, "Function block-based closed-loop adaptive machining for assembly interfaces of large-scale aircraft components," *Robot Comput Integr Manuf* **66**, 101994 (2020).
- [10] J. D. Cao, J. Z. Zhang, T. Wang, J. H. Meng, S. L. Li and M. Li, "Mechanism design and dynamic switching modal control of the wheel-legged separation quadruped robot," *Robotica* **42**(3), 660–683 (2024).
- [11] J. Zhang, M. Li, J. Cao, Y. Dou and X. Xiong, "Research on bionic jumping and soft landing of single leg system in quadruped robot," *J Bionic Eng* **20**(5), 2088–2107 (2023).
- [12] J. S. Dai and J. Rees Jones, "Mobility in metamorphic mechanisms of foldable/Erectable kinds," *ASME J Mech Des* **121**(3), 375–382 (1999).
- [13] F. Aimedee, G. Gogu, J. S. Dai, C. Bouzgarrou and N. Bouton, "Systematization of morphing in reconfigurable mechanisms," *Mech Mach Theory* **96**, 215–224 (2016).
- [14] C. Singh and G. Liu, "Energy-aware redundant actuation for safe spring-assisted modular and reconfigurable robot," *Robotica* **40**(12), 4498–4511 (2022).
- [15] H.-S. Yan and C.-H. Kang, "Configuration synthesis of mechanisms with variable topologies," *Mech Mach Theory* **44**(5), 896–911 (2009).
- [16] K. T. Zhang, J. S. Dai and Y. F. Fang, "Geometric constraint and mobility variation of two 3s(V)Ps(V) metamorphic parallel mechanisms," *ASME J Mech Des* **135**(1), 011001 (2013).
- [17] X. Ma, K. Zhang and J. S. Dai, "Novel spherical-planar and Bennett-spherical 6R metamorphic linkages with reconfigurable motion branches," *Mech Mach Theory* **128**, 628–647 (2018).
- [18] W. Ye, X. Chai and K. Zhang, "Kinematic modeling and optimization of a new reconfigurable parallel mechanism," *Mech Mach Theory* **149**, 103850 (2020).
- [19] Y. Lu, N. Ye and L. Ding, "Type synthesis of spatial 3-DoF parallel mechanisms with planar sub-chains using revised digital topological graphs and arrays," *Robotica* **35**(2), 370–383 (2017).
- [20] X. Zhang, D. Mu, Y. Zhang, H. You and H. Wang, "Type synthesis of multi-loop spatial mechanisms with three translational output parameters based on virtual-loop theory and assur groups," *Robotica* **37**(6), 1104–1119 (2019).
- [21] Y. Tian, Y. Zhao, L. Li, G. Yuan and F. Xi, "Design and analysis of a multi segment shape morphing mechanism," *J Mech Robot* **13**(2), 021004 (2021).
- [22] T. Song, H. Yang, S. Guo, G. Cui and Z. Yan, "Configuration selection for tip-over stability of a modular reconfigurable mobile manipulator under various application situations," *Robotica* **41**(3), 1066–1085 (2023).
- [23] C. Galletti and P. Fanghella, "Single-loop kinematotropic mechanisms," *Mech Mach Theory* **36**(6), 743–761 (2001).
- [24] C. Galletti and E. Giannotti, "Multiloop Kinematotropic Mechanisms," **In:** *ASME. 2002 International Design Engineering Technical Conferences and Computers and Information in Engineering Conference*, Quebec, Canada (2002) pp. 455–460.
- [25] Q. Meng, X.-J. Liu and F. Xie, "Structure design and kinematic analysis of a class of ring truss deployable mechanisms for satellite antennas based on novel basic units," *Mech Mach Theory* **174**, 104881 (2022).
- [26] C. Tian, D. Zhang, H. Tang and C. Wu, "Structure synthesis of reconfigurable generalized parallel mechanisms with configurable platforms," *Mech Mach Theory* **160**, 104281 (2021).
- [27] J. Zhang, Z. Jin and H. Feng, "Type synthesis of a 3-mixed-DOF protectable leg mechanism of a firefighting multi-legged robot based on GF set theory," *Mech Mach Theory* **130**, 567–584 (2018).
- [28] J. S. Dai, D. Li, Q. Zhang and G. Jin, "Mobility analysis of a complex structured ball based on mechanism decomposition and equivalent screw system analysis," *Mech Mach Theory* **39**(4), 445–458 (2004).
- [29] H. Ding, W.-A. Cao, Z. Chen and A. Kecskemethy, "Structural synthesis of two-layer and two-loop spatial mechanisms with coupling chains," *Mech Mach Theory* **92**, 289–313 (2015).
- [30] Q. Zeng and Y. Fang, "Structural synthesis and analysis of serial-parallel hybrid mechanisms with spatial multi-loop kinematic chains," *Mech Mach Theory* **49**, 198–215 (2012).
- [31] H. Gao, J. Liu and Y. Yu, "Design and motion analysis of a novel coupled mechanism based on a regular triangular bipyramid," *Int J Adv Robot Syst* **13**(6), 172988141667813 (2016).
- [32] C. Tian, Y. Fang and Q. J. Ge, "Structural synthesis of parallel manipulators with coupling sub-chains," *Mech Mach Theory* **118**, 84–99 (2017).
- [33] C. Tian, Y. Fang and Q. J. Ge, "Structural synthesis of a class of two-loop generalized parallel mechanisms," *Mech Mach Theory* **128**, 429–443 (2018).
- [34] C. Paul, F. J. Valero-Cuevas and H. Lipson, "Design and control of tensegrity robots for locomotion," *IEEE Trans Robot* **22**(5), 944–957 (2006).
- [35] W. A. Cao, D. Yang and H. Ding, "Topological structural design of umbrella-shaped deployable mechanisms based on new spatial closed-loop linkage units," *ASME J Mech Des* **140**(6), 062302 (2018).
- [36] J. Liu, X. Fan and H. Ding, "Investigation of a novel 2R1T parallel mechanism and construction of its variants," *Robotica* **39**(10), 1834–1848 (2021).
- [37] Y. Ju, W. Xu, G. Meng and Y. Cao, "Constraint characteristics and type synthesis of two families of 1T2R parallel mechanism," *Robotica* **40**(9), 3033–3056 (2022).
- [38] T. Demjen, E.-C. Lovasz, M. Ceccarelli, C. Sticlaru, A.-M.-F. Lupuți, A. Oarcea and D.-C. Silaghi-Perju, "Design of the five-bar linkage with singularity-free workspace," *Robotica* **41**(11), 3361–3379 (2023).
- [39] Y. Han, Q. He and B. Zheng, "Study on rubber surface enhancement of fiber fabric," *J Polym Res* **28**(3), 85(2021).
- [40] Y. Kakehashi, K. Okada and M. Inaba, "Development of Continuum Spine Mechanism for Humanoid Robot: Biomimetic Supple and Curvilinear Spine Driven by Tendon," **In:** *3rd IEEE International Conference on Soft Robotics (RoboSoft)*, New Haven, CT, USA (2020) pp. 312–317, 2020.

Appendix A. Twist/constraint wrench screw systems of RR*-UU-RR*-UU limbs

Table VII. Twist/constraint wrench screw systems of RR-UU-RR*-UU limbs.*

Decoupled limbs	Decentralized limbs	Decentralized limbs twist screw systems	Decoupled limbs twist screw systems	Decoupled limbs constraint wrench screw systems
Limb C1	Limb 1	$\$_{L11} = (0, 0, 0; d, -e, 0)$	$\$_{CL11} = (0, 0, 0; d, -e, 0)$	$\$_{CL11}^r = (0, 0, 1; -b, -a, 0)$ $\$_{CL12}^r = (e, d, 0; 0, 0, -(be + ad))$
		$\$_{L12} = (1, 0, 0; 0, 0, b)$	$\$_{CL12} = (1, 0, 0; 0, 0, b)$	
		$\$_{L13} = (0, 1, 0; 0, 0, a)$	$\$_{CL13} = (0, 1, 0; 0, 0, a)$	
		$\$_{L14} = (0, 0, 1; -b, -a, 0)$	$\$_{CL14} = (0, 0, 1; -b, -a, 0)$	
Limb C2	Limb 2	$\$_{L21} = (0, 0, 0; d, e, 0)$	$\$_{CL21} = (0, 0, 0; d, e, 0)$	$\$_{CL21}^r = (0, 0, 1; b, -a, 0)$ $\$_{CL22}^r = (e, -d, 0; dl_2, el_2, -(be + ad))$
		$\$_{L22} = (1, 0, 0; 0, 0, -b)$	$\$_{CL22} = (1, 0, 0; 0, 0, -b)$	
		$\$_{L23} = (0, 1, 0; 0, 0, a)$	$\$_{CL23} = (0, 1, 0; 0, 0, a)$	
		$\$_{L24} = (0, 0, 1; b, -a, 0)$	$\$_{CL24} = (0, 0, 1; b, -a, 0)$	
Limb C3	Limb 5	$\$_{L55} = (1, 0, 0; 0, l_2, -n_2)$	$\$_{CL25} = (1, 0, 0; 0, l_2, -n_2)$	$\$_{CL25}^r = (0, 0, 1; b, -a, 0)$ $\$_{CL26}^r = (e, -d, 0; dl_2, el_2, -(be + ad))$
		$\$_{L56} = (1, 0, 0; 0, l_2, n_2)$	$\$_{CL26} = (1, 0, 0; 0, l_2, n_2)$	
		$\$_{L57} = (0, 1, 0; -l_2, 0, m_2)$	$\$_{CL27} = (0, 1, 0; -l_2, 0, m_2)$	
Limb C3	Limb 3	$\$_{L31} = (0, 0, 0; -d, e, 0)$	$\$_{CL31} = (0, 0, 0; -d, e, 0)$	$\$_{CL31}^r = (0, 0, 1; b, a, 0)$ $\$_{CL32}^r = (e, d, 0; -dl_1, el_2, -(be + ad))$
		$\$_{L32} = (1, 0, 0; 0, 0, -b)$	$\$_{CL32} = (1, 0, 0; 0, 0, -b)$	
		$\$_{L33} = (0, 1, 0; 0, 0, -a)$	$\$_{CL33} = (0, 1, 0; 0, 0, -a)$	
		$\$_{L34} = (0, 0, 1; b, a, 0)$	$\$_{CL34} = (0, 0, 1; b, a, 0)$	
Limb C3	Limb 6	$\$_{L65} = (1, 0, 0; 0, l_1, -n_1)$	$\$_{CL35} = (1, 0, 0; 0, l_1, -n_1)$	$\$_{CL35}^r = (0, 0, 1; b, a, 0)$ $\$_{CL36}^r = (e, d, 0; -dl_1, el_2, -(be + ad))$
		$\$_{L56} = (1, 0, 0; 0, l_2, -n_2)$	$\$_{CL36} = (1, 0, 0; 0, l_2, -n_2)$	
		$\$_{L57} = (1, 0, 0; 0, l_2, n_2)$	$\$_{CL37} = (1, 0, 0; 0, l_2, n_2)$	
		$\$_{L58} = (0, 1, 0; -l_2, 0, m_2)$	$\$_{CL38} = (0, 1, 0; -l_2, 0, m_2)$	

Table VII. Continued.

Decoupled limbs	Decentralized limbs	Decentralized limbs twist screw systems	Decoupled limbs twist screw systems	Decoupled limbs constraint wrench screw systems
Limb C4	Limb 4	$\$_{L41} = (0, 0, 0; -d, -e, 0)$	$\$_{CL41} = (0, 0, 0; -d, -e, 0)$	$\$_{CL41}^r = (0, 0, 1; -b, a, 0)$ $\$_{CL42}^r = (-e, d, 0; -dl_1, -el_2, -(be + ad))$
		$\$_{L42} = (1, 0, 0; 0, 0, b)$	$\$_{CL42} = (1, 0, 0; 0, 0, b)$	
	Limb 7	$\$_{L43} = (0, 1, 0; 0, 0, -a)$	$\$_{CL43} = (0, 1, 0; 0, 0, -a)$	
		$\$_{L44} = (0, 0, 1; -b, a, 0)$	$\$_{CL44} = (0, 0, 1; -b, a, 0)$	
		$\$_{L75} = (1, 0, 0; 0, l_2, -n_2)$	$\$_{CL45} = (1, 0, 0; 0, l_2, -n_2)$	
	Limb 6	$\$_{L76} = (1, 0, 0; 0, l_2, n_2)$	$\$_{CL46} = (1, 0, 0; 0, l_2, n_2)$	
		$\$_{L77} = (0, 1, 0; -l_2, 0, -m_2)$	$\$_{CL47} = (0, 1, 0; -l_2, 0, -m_2)$	
	Limb 5	$\$_{L68} = (1, 0, 0; 0, l_1, -n_1)$	$\$_{CL48} = (1, 0, 0; 0, l_1, -n_1)$	
		$\$_{L59} = (1, 0, 0; 0, l_2, -n_2)$	$\$_{CL49} = (1, 0, 0; 0, l_2, -n_2)$	
		$\$_{L51} = (1, 0, 0; 0, l_2, n_2)$	$\$_{CL4I} = (1, 0, 0; 0, l_2, n_2)$	
Limb C5	Limb 2	$\$_{L5II} = (0, 1, 0; -l_2, 0, m_2)$	$\$_{CL4II} = (0, 1, 0; -l_2, 0, m_2)$	
		$\$_{L21} = (0, 0, 0; d, e, 0)$	$\$_{CL51} = (0, 0, 0; d, e, 0)$	
		$\$_{L22} = (1, 0, 0; 0, 0, -b)$	$\$_{CL52} = (1, 0, 0; 0, 0, -b)$	
		$\$_{L23} = (0, 1, 0; 0, 0, a)$	$\$_{CL53} = (0, 1, 0; 0, 0, a)$	
	Limb 6	$\$_{L24} = (0, 0, 1; b, -a, 0)$	$\$_{CL54} = (0, 0, 1; b, -a, 0)$	
		$\$_{L65} = (1, 0, 0; 0, l_1, -n_1)$	$\$_{CL55} = (1, 0, 0; 0, l_1, -n_1)$	
	Limb 7	$\$_{L76} = (1, 0, 0; 0, l_2, -n_2)$	$\$_{CL56} = (1, 0, 0; 0, l_2, -n_2)$	
		$\$_{L77} = (1, 0, 0; 0, l_2, n_2)$	$\$_{CL57} = (1, 0, 0; 0, l_2, n_2)$	
	Limb 8	$\$_{L78} = (0, 1, 0; -l_2, 0, -m_2)$	$\$_{CL58} = (0, 1, 0; -l_2, 0, -m_2)$	
		$\$_{L89} = (1, 0, 0; 0, l_1, n_1)$	$\$_{CL59} = (1, 0, 0; 0, l_1, n_1)$	

Table VII. Continued.

Decoupled limbs	Decentralized limbs	Decentralized limbs twist screw systems	Decoupled limbs twist screw systems	Decoupled limbs constraint wrench screw systems
Limb C6	Limb 3	$\$_{L31} = (0, 0, 0; -d, e, 0)$	$\$_{CL61} = (0, 0, 0; -d, e, 0)$	$\$_{CL61}^r = (0, 0, 1; b, a, 0)$ $\$_{CL62}^r = (e, d, 0; -dl_1, el_2, -(be + ad))$
		$\$_{L32} = (1, 0, 0; 0, 0, -b)$	$\$_{CL62} = (1, 0, 0; 0, 0, -b)$	
		$\$_{L33} = (0, 1, 0; 0, 0, -a)$	$\$_{CL63} = (0, 1, 0; 0, 0, -a)$	
		$\$_{L34} = (0, 0, 1; b, a, 0)$	$\$_{CL64} = (0, 0, 1; b, a, 0)$	
	Limb 7	$\$_{L75} = (1, 0, 0; 0, l_2, -n_2)$	$\$_{CL65} = (1, 0, 0; 0, l_2, -n_2)$	
		$\$_{L76} = (1, 0, 0; 0, l_2, n_2)$	$\$_{CL66} = (1, 0, 0; 0, l_2, n_2)$	
Limb 8	$\$_{L77} = (0, 1, 0; -l_2, 0, -m_2)$	$\$_{CL67} = (0, 1, 0; -l_2, 0, -m_2)$		
	$\$_{L88} = (1, 0, 0; 0, l_1, n_1)$	$\$_{CL68} = (1, 0, 0; 0, l_1, n_1)$		
Limb C7	Limb 4	$\$_{L41} = (0, 0, 0; -d, -e, 0)$	$\$_{CL71} = (0, 0, 0; -d, -e, 0)$	$\$_{CL71}^r = (0, 0, 1; -b, a, 0)$ $\$_{CL72}^r = (-e, d, 0; -dl_1, 0, -(be + ad))$
		$\$_{L42} = (1, 0, 0; 0, 0, b)$	$\$_{CL72} = (1, 0, 0; 0, 0, b)$	
		$\$_{L43} = (0, 1, 0; 0, 0, -a)$	$\$_{CL73} = (0, 1, 0; 0, 0, -a)$	
		$\$_{L44} = (0, 0, 1; -b, a, 0)$	$\$_{CL74} = (0, 0, 1; -b, a, 0)$	
	Limb 8	$\$_{L85} = (1, 0, 0; 0, l_1, n_1)$	$\$_{CL75} = (1, 0, 0; 0, l_1, n_1)$	

Appendix B. Nomenclatures

RrPAP	Reconfigurable redundant posture adjustment platform
WMP	Wheeled mobile platform
PAM	Posture adjustment mechanism
PM	Parallel mechanism
RPM	Redundant parallel mechanism
DLPM	Decentralized limbs parallel mechanism
3T1R	Three translations and three rotations
DOF	Degree of freedom
LN	Number of limbs
PN	Number of prismatic joints
KSN	Sum of the number of kinematic pairs
DN	Number of driving pairs
MP	Moving platform
FP	Fixed platform
VP	Virtual platform
CS	Coupling sub-chain
